

IoT SUPERVISED PV-HVDC COMBINED WIDE AREA POWER NETWORK SECURITY SCHEME USING WAVELET-NEURO ANALYSIS

Gantaiah Swamy GARIKA , Padma KOTTALA 

Department of Electrical and Electronics Engineering, Andhra University College of Engineering, Andhra University, Waltair Junction, 530003 Visakhapatnam, Andhra Pradesh, India

swamyaliet@gmail.com, padma315@gmail.com

DOI: 10.15598/aece.v20i4.4595

Article history: Received Jun 11, 2022; Revised Oct 05, 2022; Accepted Oct 25, 2022; Published Dec 31, 2022.
This is an open access article under the BY-CC license.

Abstract. Power system networks are one of the most widely used methods in the real world for transferring large amounts of electrical energy from one location to another. At present, High Voltage Direct Current Transmission is preferred for long distances over hundreds of miles due to minimal power loss and transmission cost of transmission. Due to an increase in power demand, integration of renewable sources to minimise the voltage fluctuations and compensate for power loss is necessary. This is a mandatory requirement to produce sophisticated protection methods for mainly smart systems under various balanced and unbalanced fault conditions. The system protection scheme must respond as quickly as possible to protect the connected devices in a smart environment. The network must be monitored and protected under various weather conditions as well as electrical parametric problems. The proposed research work is carried on the basis of physical monitoring with the aid of the Internet-of-Things and electrical parameters calibrated with the help of wavelet analysis. A wavelet is a mathematical tool to investigate the behaviour of transient signals at different frequencies, which provides important information related to the detailed analysis of faults in power networks. The major goals of this research are to analyse faults using detailed coefficients of current signals through the bior-1.5 mother wavelet for fault identification and artificial neural network analysis for fault localization. This proposed approach furnishes an IoT supervised Photovoltaic - High Voltage Direct Current (HVDC) combined wide area power network security scheme using wavelet detailed coefficients under various types of faults with Fault-Inception-Angles.

Keywords

Fault detection, HVDC, Internet of Things (IoT), Neural Networks, PV Energy Source, Wavelet Transform.

1. Introduction

The power network plays a major role in connecting various electrical power devices and transferring power from a source to different locations. The transmission lines are delivering large amounts of power to load distribution centres and then end consumers, moving power from one place to other parts of the country [1]. The high-tension line imports extensive power and could transfer several miles. Most of the power lines are unprotected in poor weather conditions and are exposed to falling objects that may damage the lines and also disturb the power transmission. It may cause difficulty in supplying extended power to consumers. It can be prevented by disconnecting defective equipment from the power network by designing a proper security system with a power electronic switching mechanism [2].

Transmission line protection is basically distance protection and is based on impedance calculation at the relay point. This type of protection has several drawbacks [3] due to the wrong operation of relays tripping at temporary faults, power swings, and overloading conditions, and it may lead to blackouts in the system network. So, it is necessary to think about alternative methods to protect electrical elements kept

in safe mode. The scheme requires minimising detection time quantum and then isolating faulty equipment from the existing system [4]. A fast-acting relay mechanism is required to isolate the defective equipment from the electric network.

The above problem can be solved by making use of digital communication and global synchronisation [5] and [6]. In the present scenario, the electrical protection schemes are looking for electrical problems only, but the problems may arise due to mechanical damage. The system must be protected from electrical as well as mechanical damage by clear monitoring of connected devices. The system can be monitored by means of IoT devices, which are operated in parallel with electrical circuit parameters. The IoT monitored network is capable of developing a predominant protection scheme for electrical as well as mechanical problems.

The IoT technologies are related to broad band, Global System for Mobile Communications (GSM), General Packet Radio Service (GPRS), and Zigbee, which cover up to a range of a few kilometres due to the lack of data [7]. The technological difficulties in using traditional protection methods and the requirement for an intelligent, adaptable protection solution. However, building a dependable adaptive protection mechanism is still difficult due to the danger of communication connection failures and cyber security threats. A backup plan is required when a communication problem prevents the relay from switching to a lower current level during disconnected mode [8].

Microgrids have problems, such as sympathetic tripping and protection blindness. The way that microgrids function is different from that of the traditional electricity system. Micro-grids can run in either an islanded mode or a grid-connected mode. Microgrids use energy storage technologies and dispersed renewable energy sources like solar and wind in the "island" mode. Both situations put the system's modes up against obstacles like short circuit current in power electronic interface production or protection blinding [9]. High Voltage Direct Current (HVDC) transmission has some superior advantages to Alternating Current (AC) applications, for instance, huge amounts of power for long distances, AC interconnection stability, long underground cabling, and minimising losses and transportation costs [10].

A Static-Var-Compensator (SVC) is based on a Thyristor-Controlled-Reactor (TCR), a Thyristor-Switched-Capacitor (TSC), and/or a Fixed-Capacitor (FC) tuned to filters integrated with an off-shore Wind-Farm (WF) Analytical results are verified and presented on a simulation platform that compares under-reach phenomena in the presence of Flexible AC Transmission Systems devices, and it is found that

under-reach is more severe for SVC connected systems [11].

Modern power lines require fast detection and location of faults. At present, Artificial Intelligence techniques are used to find the problem in the system by calibrating the data with a minimum number of calculations. One of the tools for detecting and discriminating the fault in the protection scheme has been presented in [12] with the support of phase current and voltages. In transmission, there are primarily two types of faults: symmetrical and unsymmetrical, which are classified as 1-Ph, 2-ph, and 3-phG. They fall under the category of unsymmetrical faults, while 3-ph faults under the category of symmetrical faults, as do open circuit faults.

The Biorthogonal wavelet family demonstrates the linear phase property, which is required for signal and image reconstruction. Interesting qualities are produced by utilising two wavelets instead of only one, one for decomposition and the other for reconstruction. After extensive testing, the bior-1.5 mother wavelet's property has proven to be suitable for fault analysis. The proposed algorithm establishes a security system for IoT-PV Integrated wide area power system protection in the presence of HVDC supplementary control using wavelet study is used with bior-1.5 mother-wavelet approximate and detailed-coefficients. This research method can interact with digital relays and then isolate faulty elements faster than previous popular schemes.

2. System Study and Numerical Modeling

The growth of energy requirements is due to population and mechanization. It is a mandatory prerequisite to search for alternate energy sources to diminish the shortage of electrical demand supply by injecting renewable energy sources into the network. Solar energy is an attractive source compared to all other non-conventional sources. The solar plant comprises a DC-DC boost converter, and another one is a voltage source converter (VSC), which can control and convert DC-to-AC power [13]. At present, HVDC is preferred for long distances over hundreds of miles due to minimising power loss and transmission cost of transmission. HVDC grids can be joined to VSC-HVDC networks in a mesh network just as readily as regular AC grids. Compared to two-level VSC configurations, the modular multilevel converter is more effective [14]. The following sections report on proposed system component modeling.

2.1. Solar Photovoltaic Modeling

The generation of electrical power by arranging PV cells in parallel and series combination groups to get the required current and voltage level. The circuit diagram of the PV module is expressed in Fig. 1. The modelling of the solar photovoltaic control structure and its components is illustrated in Fig. 2. The current-voltage parameter can be characterised by the mathematical statements as follows:

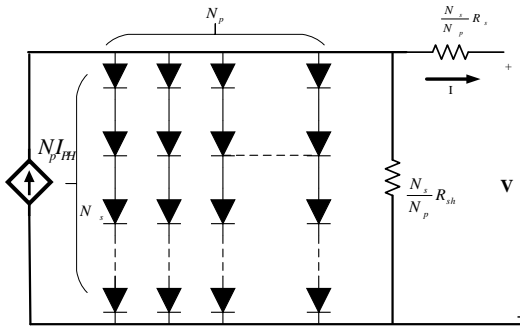


Fig. 1: Circuit model of photo voltaic module.

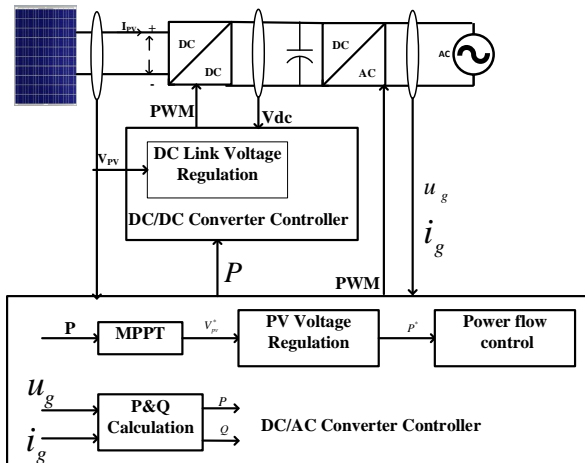


Fig. 2: Modeling of solar photo voltaic control structure.

The current-voltage parameter can be characterised by the mathematical statements as follows:

$$I_{ph} = [I_{sc} + K_i (T - 298)] \cdot \frac{I_r}{1000}. \tag{1}$$

The module Reverse saturation current is:

$$I_{rs} = \frac{I_{sc}}{\left[e^{\left(\frac{qV_{OC}}{N_s k n T} \right)} - 1 \right]}. \tag{2}$$

The specified notations as follows: V_{OC} - open circuit voltage in volts, N_s - Number of series cells connected,

(I_{ph}) - Photon-current, (I_{sc}) - short-circuit-current, k - Boltzmann's constant, T - temperature.

Module saturation current with varying temperature can be calculated using following equation:

$$I_0 = I_{rs} \left[\frac{T}{T_r} \right]^3 e^{\left[\frac{q \cdot E_{g0}}{n k} \left(\frac{1}{T} - \frac{1}{T_r} \right) \right]}. \tag{3}$$

The output current of PV module is defined as:

$$I = N_p \cdot I_{ph} - N_p \cdot I_0 \left[e^{\left(\frac{V + I \cdot R_s}{n \cdot V_t} \right)} - 1 \right] - I_{sh}, \tag{4}$$

where number of PV modules are connected in parallel (N_p), shunt and series resistances (R_{sh}) and (R_s) is measured in Ω .

$$v_t = \frac{k \cdot T}{q}, \tag{5}$$

$$I_{sh} = \frac{V \cdot \frac{N_p}{N_s} + I \cdot R_s}{R_{sh}}. \tag{6}$$

2.2. HVDC Transmission

The majority of power must currently be delivered across larger distances because of the daily rise in energy demand. It is necessary to think about reducing the cost of generation, transmission, and distribution. The cost reduction can only be achieved by reducing the cost of generation by setting up remote generating stations. Since the majority of the power is hundreds of kilometres away from the load distribution centers, the transmission costs may rise. The problem associated with AC power at high voltages may lead to additional costs due to active and reactive power compensating devices. It is necessary to search for alternative solution to minimise the cost of transmission. On the present trend, one of the alternative sources is HVDC [15]. It has many benefits over AC transmission, such as stability, voltage and current limits, active and reactive power control, harmonics and economic factors, etc. The most cost-effective method for long-distance bulk power transmission is the Voltage Source Converter (VSC) based High Voltage Direct Current (HVDC) connection, which is used to connect distributed generating sources into AC grids [16].

Figure 3 illustrates the High Voltage Direct Current (HVDC) system block diagram, which consists of two converters with constant excitation controllers and constant current controllers adjusted with ignition angle α . The converter's operation depends on the ignition angle α . The DC output voltage is positive when

$\alpha < 90^\circ$ and it operates as a rectifier. The output voltage is negative when $\alpha < 90^\circ$ and it operates as a converter. The HVDC link converter power flow can be either DC/AC or AC/DC as per the operation of the inverter or converter [17]. The converter DC voltage can be expressed as:

$$V_{dr} = \frac{V_{d0}}{2} [\cos(\alpha + \mu)], \tag{7}$$

$$I_d = I_{SC} [\cos \alpha - \cos(\alpha + \mu)], \tag{8}$$

where V_{d0} known as DC output voltage and is represented as $V_{d0r} = \frac{3\sqrt{3}}{\Phi} E_m$, The equivalent AC and DC power is represented as follows:

$$3V I_L \cos \Phi = V_d I_d = I_d V_{d0} \cos \alpha. \tag{9}$$

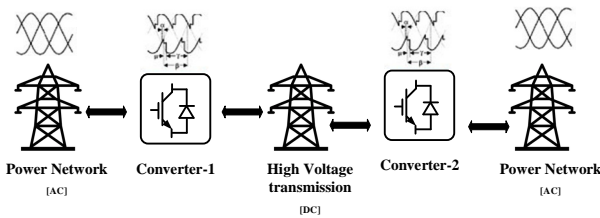


Fig. 3: High Voltage Direct Current (HVDC) system block diagram.

The inverter operation equations are changed by changing sign of DC voltage V_d and $\cos \alpha = -\cos \beta$ and also $\cos \delta = -\cos \gamma$. Then, the converter operates as inverter and also power flow will change direction.

$$V_{di} = -\frac{V_{d0}}{2} [\cos \gamma + \cos \beta], \tag{10}$$

$$I_d = I_{SC} [\cos \gamma - \cos \beta]. \tag{11}$$

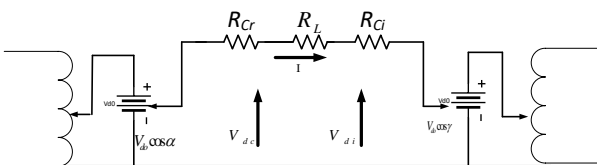


Fig. 4: Steady state simulation circuit of HVDC.

$$I_d = \frac{V_0 \cos \alpha - V_0 \cos \beta \text{ or } \delta}{R_{Cr} + R_l \pm R_{Ci}}. \tag{12}$$

The controller can have the flexibility to operate as a rectifier or converter. The schematic diagram of converters is shown in Fig. 4. The HVDC link includes two converters; both will have Constant Excitation Angle control (CEA) and Constant Current (CC) control [18]. The controllers in converters provide the flexibility for the operation of either rectifier or inverter, and the arrangement of converter controllers is as shown in Fig. 5.

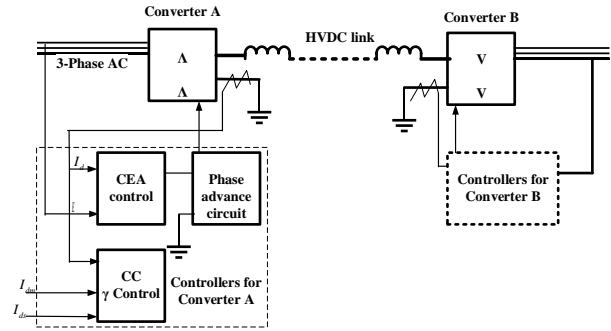


Fig. 5: Schematic arrangement of converter controllers for an HVDC Link.

3. Power System Security With IoT

When considering the probability of changes to the system (contingencies) and its surroundings, one way to define power system security is the likelihood that the operating point of the system will remain within acceptable bounds.

The time determinism and refresh rate that are unique to Phasor Measurement Units (PMU)-based state estimation procedures for active distribution networks allow them to meet the time-critical protection needs as well as the accuracy standards imposed by faulty line identification [19]. Power system stability during transients is crucial. In order to reestablish transient stability, large disturbances, such as transmission line faults, are a worry that must be detached as soon as possible. The location, detection, and classification of defects in a transmission network are all done using faulty current and voltage signals [20]. The circuit breaker isolates the unhealthy transmission line from the rest of the health system after the relay identifies an irregular signal.

The intended method employs a post-fault single-cycle current waveform, and wavelet packet transform is used to preprocess the data. From the decomposed coefficients, energy and entropy are calculated, and a feature matrix is created. The forward feature selection approach is then used to remove and normalise the redundant features from the matrix. By taking into account the factors from a simulation environment, such as fault type, resistance path, inception angle, and distance, test and train data are created. Support vector machines that have had their parameters improved using the particle swarm approach are used to analyse the test data [21].

The Internet of Things is widely employed in a range of applications, including smart energy monitoring and industrial automation. The IoT devices are used at different phases of the Smart Grid (SG) to track grid

statistics and control them for safe and effective power distribution. Although the IoT integration in the SG area has numerous advantages, it nevertheless faces some difficulties that must be overcome for the grid to operate well [22] and [23]. Figure 6(a) and Fig. 6(b) show the basic architecture of the IoT in power system protection applications.

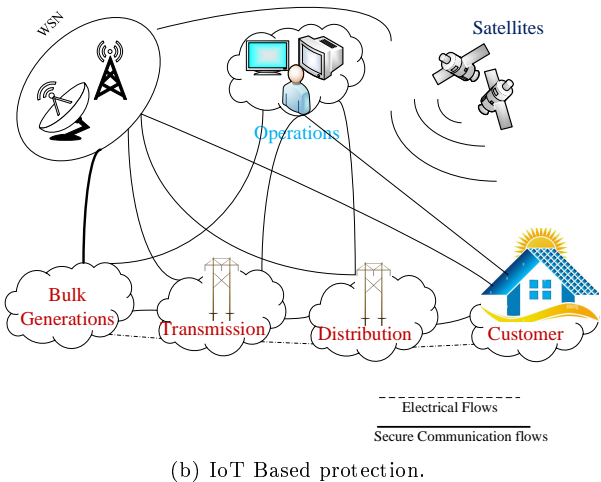
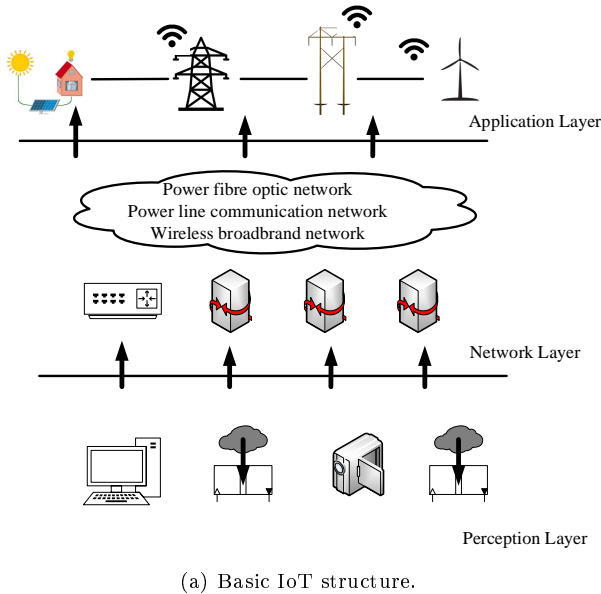


Fig. 6: IoT aided power system network.

This IoT system contains various sensors that generate early warning signals and alert control centres about the electrical and mechanical conditions of the system [24]. Figure 6(a) depicts the basic IoT structure. The IoT-based transmission system protection incorporates mechanical and electrical safety of power lines as illustrated in Fig. 6(b).

The Wavelet Transform (WT) is a popular mathematical tool to analyse transient signal provides detailed information about fault detection and discrimination [25] and [26]. The disturbances are

calibrated by means of ANN training patterns, which are generated from wavelet coefficients extracted from current wave forms [27] and [28] using certain measuring devices. The indices of the sampling current signals are supplied to the ANN module, which then finds the fault distance. The procedural operation is represented in Fig. 5.

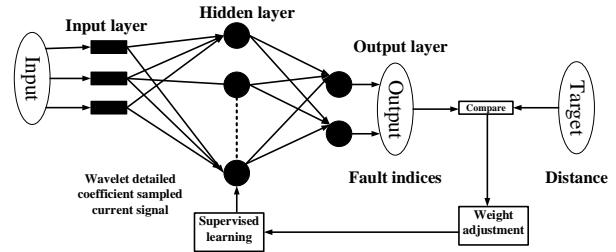


Fig. 7: Diagrammatic representation of Neuro wavelet based security scheme.

4. System Study and methodology

The proposed system is a 230 kV wide area network that contains two utility grids, two photovoltaic energy sources each of 100 MW, and an HVDC link with voltage source converters is connected in between Bus-7 and Bus-9 and six-zones are illustrated in Fig. 8 and the system dimensions are expressed in Tab. 1 and Tab. 2.

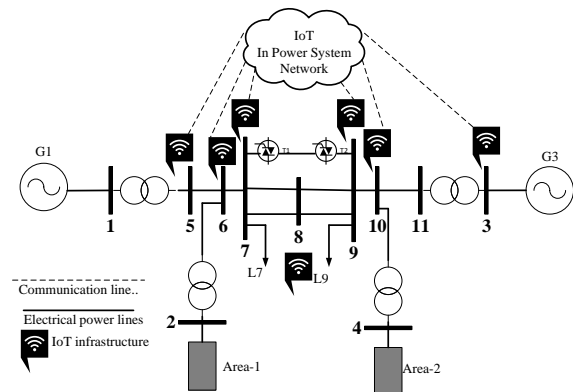


Fig. 8: Proposed two area power network test system.

Tab. 1: Parameters of the proposed system.

T-1&3	Utility Grid, 230 kV
T-2&4	Wind Energy source, 100 MW _P
T-line	$R = 0.01273 \Omega \cdot \text{km}^{-1}$, $R0 = 0.3864 \Omega \cdot \text{km}^{-1}$, $L = 0.9337 \cdot 10^{-3} \text{ H} \cdot \text{km}^{-1}$, $L0 = 4.1264 \cdot 10^{-3} \text{ H} \cdot \text{km}^{-1}$, $C = 12.74 \cdot 10^{-9} \text{ F} \cdot \text{km}^{-1}$, $C0 = 7.751 \cdot 10^{-9} \text{ F} \cdot \text{km}^{-1}$,

T-1&3: Terminal 1 and 3, T-2&4: Terminal 2 and 4, T-line: Transmission Line.

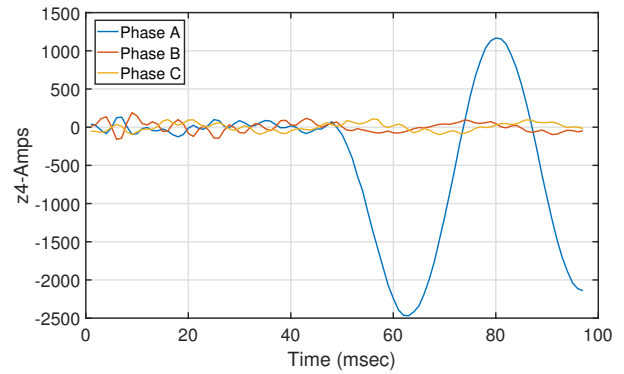
Tab. 2: Transmission line zones description.

Total Transmission Line Length : 270 km		
Area-I		
	line Section between	Line Length
Zone-1	Bus-5 & Bus-6	25 km
Zone-2	Bus-6 & Bus-7	10 km
Zone-3	Bus-7 & Bus-8	110 km
Area-II		
Zone-4	Bus-8 & Bus-9	110 km
Zone-5	Bus-9 & Bus-10	10 km
Zone-6	Bus-10 & Bus-11	25 km

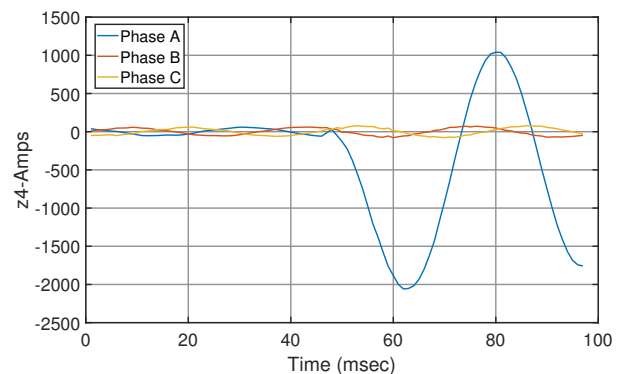
5. Results and Discussions

The main cases studied in the research work are fault classification, varying faults at different distances, and fault inception angles. The selection of sampling frequency is important due to deep analysis under various fault inception angles. The wave form analysis is calibrated at the frequency of 60 Hz, 32 sections for 1 cycle, and every section has 100 points considered, i.e. $60 \cdot 32 \cdot 100 = 192,000$ simulations considered for every type of fault and fault inception angle combination. The fault intolerance and location can be calculated by the use of wavelet detailed coefficients of the current signal with and without HVDC Link. The fault analysis can be carried out by comparing phase currents, which have higher values compared to healthy phase currents observed in Fig. 9.

The impact of HVDC is observed from Fig. 10(a) and Fig. 10(b), which indicate that the amplitude of current signal is decreased due to HVDC integration. The impact of the HVDC link can be compared with the support of Fig. 9 and Fig. 10. The fault current amplitude of the HVDC integrated system is less than that of a normal PV system. The detection of faults is observed with the analysis of every zone's current signal values from zone-1 to zone-6. The detailed coefficients of every zone are calibrated to find the fault in the zone. It is noted that index values are higher when compared to all the index values. The fault is then identified as SLG, DLG, or TLG faults.



(a) Solar Energy Connected system.



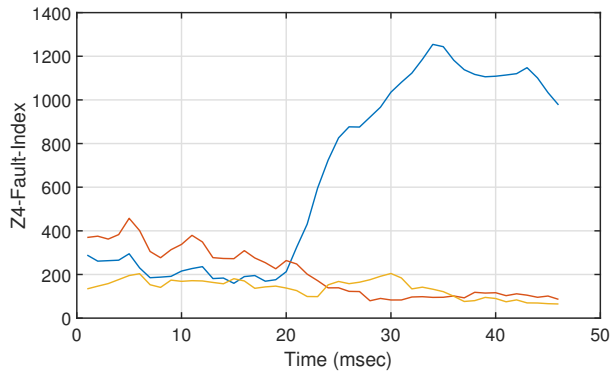
(b) PV and HVDC combined system.

Fig. 9: Current waveform for AG fault at Zone-3 in Area-1.

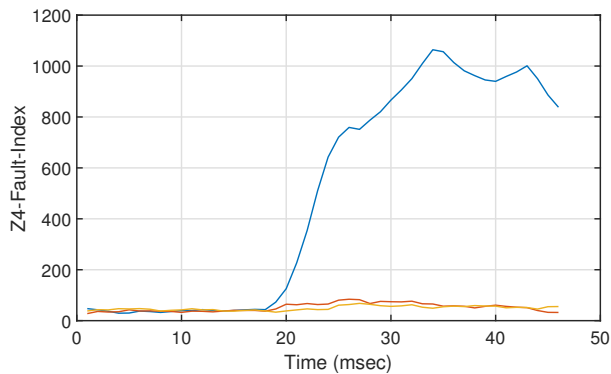
The fault analysis was carried at different distances with and without the HVDC linked solar-PV system shown in Fig. 11. The algorithm proved that the type of fault can be found irrespective of distance and fault inception angle. The sum of the detailed coefficients of various zones of current signal illustrates that the fault is more visible with a short duration of time as presented in Fig. 10, which is less quantum time when compared to normal current signal analysis with fault index, which is generated from sum-of-detailed coefficients.

The impact of fault analysis at the time of HVDC integration is calibrated using Support Vector Machine. Their parameters are improved using a wavelet approach to analyse the test data, which is displayed in Fig. 12.

At a frequency of 50 Hz, line currents I_a , I_b , and I_c at a frequency of 50 Hz are measured at the sending end of the line to classify the types of the fault among LG, LL, LLG, LLL, and healthy (normal) conditions. These current signals are being decomposed into nine levels using the MRA algorithm. Since, for N-level decomposition, $2N$ samples are required. The current signals with 1920 samples at a sampling period of T_s of $5.208 \cdot 10^{-5}$ sec are used in this work. The input contains 1920 samples, which are passed through



(a) Solar Energy Connected system.



(b) PV and HVDC combined system.

Fig. 10: Current waveform for AG fault at Zone-3 in Area-1.

HPF and LPF, and the corresponding approximate and detailed coefficients are recorded. The high-frequency noise signals are filtered, and the corresponding first-level detailed wavelet coefficients of the bior-1.5 mother wavelet are calculated to know the fault current signal.

The data sets generated using MATLAB are made by taking into account various operating conditions, i.e., various inception angle values ranging from 0 to 180° and various fault distances from 0 to 110 km as follows:

Types of faults: AG, BG, CG, ABG, BCG, CAG, AB, BC, CA, and ABC,

Locations of faults: 10, 20, 30, 40, etc (in 10-km increments),

Angle of fault initiation:

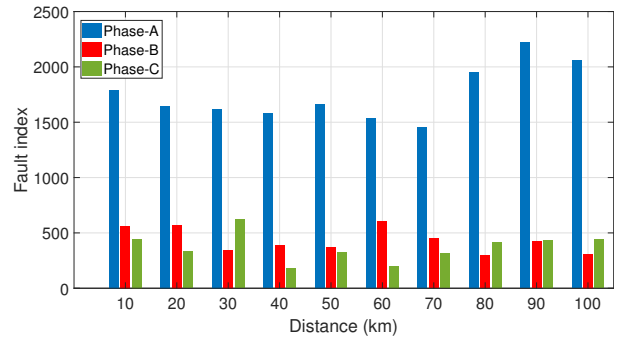
Training: 0, 20, 40, 60, and 160 (in 20-step increments),

Testing: 0, 2, 4, ... (in steps of 2).

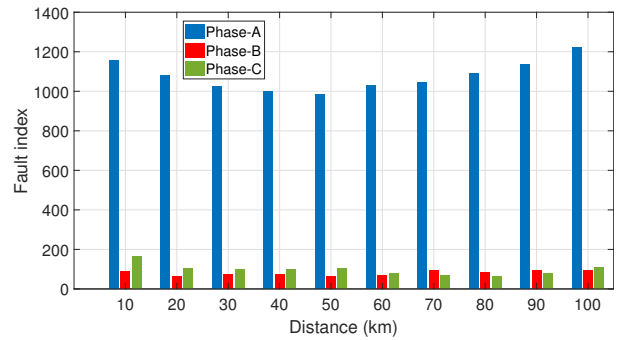
For an LG, LLG and LLLG fault, D_1 decomposition of any one faulty phase can be used to estimate fault location.

The details of the ANN architecture described as follows:

Input layer: Detail D_1 coefficients of current signals using bior-1.5 wavelets at both the ends are used



(a) Solar Energy connected system.



(b) PV and HVDC Combined system.

Fig. 11: Impact evaluation of the HVDC integrated system fault at different Distances.

location of fault,

Number Layers: two,

Number of neurons: 18,

Transfer function: Log-Sigmoid.

The comparative study investigation is performed under individual distances and FIA and establishes the relationship between the present and absent HVDC link in the network from Fig. 11. All the faulty phase values are above and below the predefined threshold value.

$$Error = \frac{ALL - CLL}{TLL} \cdot 100, \quad (13)$$

where ALL - Actual Line Length, CLL - Calculated Line Length, TLL - Total Line Length.

The analysis of the PV-HVDC integrated system under AG fault at zone-4 & Zone-3 is reported in Tab. 3 at various distances and different fault-inception-angles. The location of the fault is determined using ANN training data and detailed coefficients, then compared to the actual fault distance, finally the error is calculated. The results are presented in Tab. 4.

The sample code for testing of the proposed system with and without HVDC through a simulation model is represented in App. A.

Tab. 3: Fault analysis of PV & HVDC-PV integrated system.

	PV Integrated System					HVDC-PV Integrated System				
	Ph-A:Fault-Inception-Angle					Ph-A:Fault-Inception-Angle				
Distance	0	30	45	90	105	0	30	45	90	105
10	1650.14	1642.51	1793.91	1519.37	1439.75	1041.99	1237.87	1154.80	1137.58	1000.51
20	1619.49	1526.45	1645.86	1564.70	1311.21	957.11	1169.35	1081.45	1038.01	922.99
30	1560.16	1370.07	1620.39	1660.25	1419.21	900.83	1088.57	1023.12	990.43	884.55
40	1637.27	1462.56	1580.58	1560.16	1561.25	880.22	1060.57	999.04	968.75	870.55
50	1381.39	1425.13	1663.91	1684.76	1662.23	883.14	1046.88	985.77	956.40	860.61
60	1374.72	1197.96	1540.11	1515.29	1638.82	892.57	1076.59	1029.28	990.45	886.80
70	1780.13	1409.31	1457.74	1274.36	1047.67	880.44	1066.00	1044.04	1005.19	916.76
80	2185.44	1957.10	1952.65	1907.39	1752.97	935.21	1156.28	1092.72	1050.40	977.80
90	1747.47	1893.85	2221.43	1927.68	1597.97	966.58	1185.51	1138.33	1114.03	1033.37
100	1733.24	2062.40	2056.96	2214.33	2281.94	1157.30	1286.29	1221.46	1233.50	1199.99

	Ph-A:Fault-Inception-Angle					Ph-A:Fault-Inception-Angle				
Distance	0	30	45	90	105	0	30	45	90	105
10	647.781	509.969	560.559	381.926	491.071	185.615	138.413	86.050	74.363	47.838
20	467.788	481.508	572.415	555.882	473.964	173.945	111.165	64.187	74.092	68.975
30	303.110	316.930	344.982	389.483	366.614	168.770	103.477	71.082	85.081	89.801
40	556.246	569.134	384.880	318.272	210.159	158.837	111.176	74.677	96.841	90.736
50	387.683	399.847	368.684	350.622	234.924	127.838	95.466	65.117	86.409	89.228
60	693.489	693.096	607.852	551.401	284.571	106.351	85.839	67.227	92.425	91.907
70	627.744	562.212	450.315	381.717	427.031	90.491	91.545	91.399	113.148	95.427
80	562.961	450.169	294.015	223.278	212.016	84.518	81.886	84.458	112.282	105.649
90	681.563	586.145	423.435	341.129	371.799	90.276	98.266	92.963	102.948	101.274
100	533.944	443.819	308.921	291.761	283.852	44.162	80.506	91.466	86.431	73.813

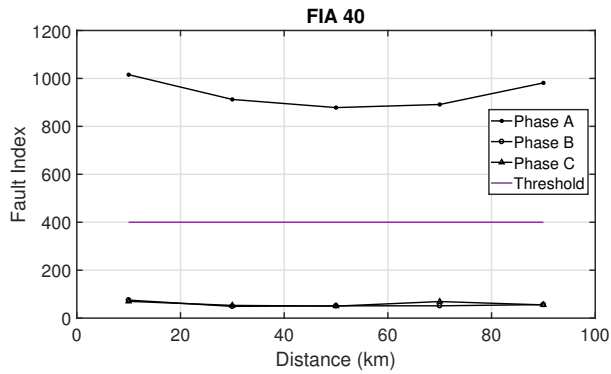
	Ph-A:Fault-Inception-Angle					Ph-A:Fault-Inception-Angle				
Distance	0	30	45	90	105	0	30	45	90	105
10	859.603	600.857	445.930	210.838	228.589	141.969	187.268	166.467	146.691	126.986
20	576.560	451.488	331.417	340.686	326.269	115.215	124.885	106.219	102.466	87.364
30	569.749	591.446	619.929	536.321	539.440	144.857	139.283	99.394	92.139	70.429
40	180.896	161.220	179.048	240.473	382.132	147.604	145.128	99.255	73.721	65.161
50	358.440	371.499	324.534	310.811	350.980	180.509	160.189	103.912	88.105	78.114
60	490.198	386.190	201.279	238.998	359.088	187.036	142.002	79.611	75.552	74.067
70	428.720	392.557	313.717	376.050	326.970	183.834	141.540	69.553	55.044	62.888
80	521.480	466.284	418.817	467.344	411.196	200.696	147.511	63.115	53.884	55.525
90	532.064	545.930	437.037	507.874	400.200	191.761	141.893	76.321	74.920	66.208
100	503.684	497.388	440.765	473.102	655.835	269.926	185.143	110.545	122.653	82.271

Tab. 4: Error analysis of fault location established on ANN algorithm at Zone-3 & Zone-4.

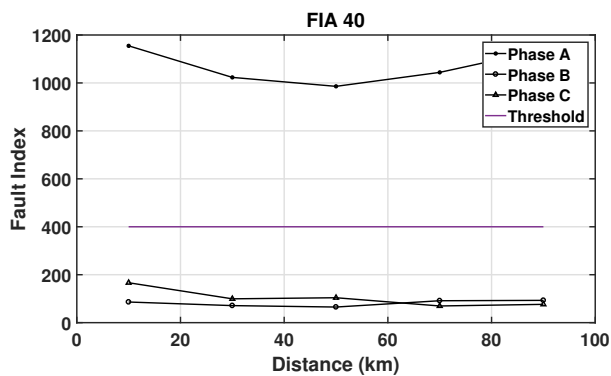
	Fault Type at zone:3						Fault Type at zone:4					
	L-G		L-L-G		L-L-L-G		L-G		L-L-G		L-L-L-G	
	AD	CD	%E	CD	%E	CD	%E	CD	%E	CD	%E	CD
20	20.04	-0.04	19	0.9	19.38	0.55	18.62	1.25	20.07	-0.06	19.78	0.2
30	30.55	-0.5	29.42	0.52	29.81	0.17	31.2	-1.09	30.11	-0.1	31.05	-0.95
40	40.11	-0.1	42.47	-2.24	43.02	-2.74	41.63	-1.48	43.78	-3.43	39.13	0.79
50	50.44	-0.4	51.4	-1.27	49.78	0.19	48.69	1.19	48.47	1.39	50.56	-0.5
60	59.01	0.89	61.52	-1.38	62.64	-2.4	63.49	-3.17	59.01	0.9	58.43	1.42
70	72.13	-1.93	69.25	0.67	69.02	0.88	66.63	3.06	69.35	0.59	70.39	-0.35
80	79.62	0.34	79.25	0.68	80.43	-0.39	80.78	-0.7	82.14	-1.94	79.54	0.41
90	89.39	0.55	91.53	1.38	91.86	-1.69	89.79	0.19	88.44	1.41	92.55	-2.31
100	99.68	0.28	99.65	0.31	100	-0.03	99.43	0.51	98.43	1.42	103.14	-2.85

AD-Actual Distance

CD-Calculated distance



(a) Solar Energy Connected system.



(b) PV and HVDC combined system.

Fig. 12: Impact evaluation of the HVDC integrated system fault at different FIA.

6. Conclusion

Power can be transmitted through an electrical network from a source to different destinations over thousands of kilometres. There is a mandatory requirement to investigate sophisticated protection methods for smart systems that depend on operational mode, transmission, and distribution under various balanced and unbalanced fault conditions. The system protection scheme must respond as quickly as possible to protect the connected devices in a smart environment.

The primary goal of the research work is to reduce detection time at the time of distinct faults. The protection schemes must concentrate not only on electrical parameters but also on the mechanical parameter calibrations due to physical and natural disasters as well as electrical load fluctuations and faults. The fault detection time quantum is reduced at the time of fault in the system when compared to normal current signal analysis with a fault index, which is generated from sum of detailed coefficients. The impact of fault analysis at the time of HVDC integration is calibrated using Support Vector Machine.

The proposed research work is carried on the basis of physical monitoring with the aid of Internet-

of-Things and electrical parameters calibrated with the help of wavelet analysis to investigate the behaviour of transient signals at different frequencies, which provides important information related to detailed analysis of faults in the power networks. This suggested algorithm presents an analysis of wavelet-based analysis of IoT-PV Energy Source Integrated Wide Area Power System Protection in the presence of HVDC supplementary control.

Author Contributions

G.S.G. developed carried out the literature survey, system simulation model design and theoretical calculations. P.K. contributed to the analysis of the results, provided critical feedback, helped to shape the research work carried out under her supervision and then verified the final version of the manuscript.

References

- [1] PRAKASH, K., A. LALLU, F. R. ISLAM and K. A. MAMUN. Review of Power System Distribution Network Architecture. In: *2016 3rd Asia-Pacific World Congress on Computer Science and Engineering (APWC on CSE)*. Nadi: IEEE, 2016, pp. 124–130. ISBN 978-1-5090-5753-5. DOI: 10.1109/APWC-on-CSE.2016.030.
- [2] JIYA, I. N. and R. GOUWS. Overview of Power Electronic Switches: A Summary of the Past, State-of-the-Art and Illumination of the Future. *Micromachines*. 2020, vol. 11, iss. 12, pp. 1–29. ISSN 2072-666X. DOI: 10.3390/mi11121116.
- [3] BO, Z. Q., X. N. LIN, Q. P. WANG, Y. H. YI and F. Q. ZHOU. Developments of power system protection and control. *Protection and Control of Modern Power Systems*. 2016, vol. 1, iss. 1, pp. 1–8. ISSN 2367-0983. DOI: 10.1186/s41601-016-0012-2.
- [4] BO, Z. Q., B. H. ZHANG, X. Z. DONG, J. H. HE. The Development of Protection Intellectuation and Smart Relay Network. *Power System Protection and Control*. 2013, vol. 41, iss. 2, pp. 1–12. ISSN 1674-3415.
- [5] DENG, X., R. YUAN, T. LI, W. LIU, Y. SHEN and Z. XIAO. Digital differential protection technique of transmission line using instantaneous active current: theory, simulation and experiment. *IET Generation, Transmission & Distribution*. 2015, vol. 9, iss. 11, pp. 996–1005. ISSN 1751-8695. DOI: 10.1049/iet-gtd.2014.0317.

- [6] SCHWEITZER, E. O., K. BEHRENDT, T. LEE, and D. A. TZIOUVARAS. Digital communications for power system protection: security, availability, and speed. In: *2001 Seventh International Conference on Developments in Power System Protection (IEE)*. Amsterdam: IET, 2001, pp. 94–97. ISBN 0-85296-732-2. DOI: 10.1049/cp:20010108.
- [7] MACHIDON O.M., C. STANCA, P. OGRUTAN, C. GERIGAN and L. ACIU. Power-system protection device with IoT-based support for integration in smart environments. *PLOS ONE*. 2018, vol. 13, iss. 12, pp. 1–22. ISSN 1932-6203. DOI: 10.1371/journal.pone.0208168.
- [8] HABIB, H. F., C. R. LASHWAY and O. A. MOHAMMED. On the Adaptive Protection of Microgrids: A Review on How to Mitigate Cyber Attacks and Communication Failures. In: *IEEE Industry Applications Society Annual Meeting*. Miami: IEEE, 2017, pp. 1–8. ISBN 978-1-5090-4894-6. DOI: 10.1109/IAS.2017.8101886.
- [9] BALASUBRAMANIAN, S., J. P. ROSELYN and K. S. SRIVIDYA. Adaptive Central Control Scheme and Investigation of Fault Current Contribution for Protection of Microgrid. *Journal of Physics: Conference Series*. 2022, vol. 2335, iss. 1, pp. 1–15. ISSN 1742-6596. DOI: 10.1088/1742-6596/2335/1/012048.
- [10] KUMAR, A. and D. M. A. HUSSAIN. HVDC (High Voltage Direct Current) Transmission System: A Review Paper. *Gyancity Journal of Engineering and Technology*. 2018, vol. 4, iss. 2, pp. 1–10. ISSN 2456-0065. DOI: 10.21058/gjet.2018.42001.
- [11] MANJUSREE, Y. and R. K. GOLI. Integration of PV and Wind Energy System with SVC for Protection of a Five Terminal Transmission Line using Wavelet Approach. *International Journal of Institutional Industrial Research*. 2018, vol. 3, iss. 1, pp. 54–60. ISSN 2456-1274. DOI: 10.21058/gjet.2018.42001.
- [12] SHERIN, T. and T. JAIMOL. HVDC Transmission Line Protection Based on Transient Power. *Procedia Technology*. 2016, vol. 25, iss. 1, pp. 660–668. ISSN 2212-0173. DOI: 10.1016/j.protcy.2016.08.158.
- [13] VINOD, R. KUMAR and S. K. SINGH. Solar photovoltaic modeling and simulation: As a renewable energy solution. *Energy Reports*. 2018, vol. 4, iss. 1, pp. 701–712. ISSN 2352-4847. DOI: 10.1016/j.egy.2018.09.008.
- [14] MITRA, B., B. CHOWDHURY and M. MANJREKAR. HVDC transmission for access to offshore renewable energy: a review of technology and fault detection techniques. *IET Renewable Power Generation*. 2018, vol. 12, iss. 13, pp. 1431–1580. ISSN 1752-1424. DOI: 10.1049/iet-rpg.2018.5274.
- [15] JOVICIC, D. and K. AHMED. *High Voltage Direct Current Transmission: Converters Systems and DC Grids*. 1st ed. Hoboken: John Wiley & Sons, 2015. ISBN 978-1-118-84666-7.
- [16] TALE, S., M. MOHAN and K. P. VITTAL. Performance analysis of distance relay in an AC grid with VSC-HVDC connection. In: *2017 International Conference on Intelligent Computing, Instrumentation and Control Technologies (ICICT)*. Kerala: IEEE, 2017, pp. 1363–1368. ISBN 978-1-5090-6106-8. DOI: 10.1109/ICICT1.2017.8342768.
- [17] MUNIAPPAN, M. A comprehensive review of DC fault protection methods in HVDC transmission systems. *Protection and Control of Modern Power Systems*. 2021, vol. 6, iss. 1, pp. 1–20. ISSN 2367-0983. DOI: 10.1186/s41601-020-00173-9.
- [18] KIM, C.-K., V. K. SOOD, G.-S. JANG, S.-J. LIM and S.-J. LEE. *HVDC Transmission: Power Conversion Applications in Power Systems: Control of HVDC Converter and System*. 1st ed. Hoboken: John Wiley & Sons, 2009. ISBN 978-0-470-82297-5.
- [19] PIGNATI, M., L. ZANNI, P. ROMANO, R. CHERKAoui, M. PAOLONE. Fault Detection and Faulted Line Identification in Active Distribution Networks Using Synchrophasors-Based Real-Time State Estimation. *IEEE Transactions on Power Delivery*. 2017, vol. 32, iss. 1, pp. 381–392. ISSN 1937-4208. DOI: 10.1109/TPWRD.2016.2545923.
- [20] MISHRA, D. P. and P. RAY. Fault detection, location and classification of a transmission line. *Neural Computing and Applications*. 2018, vol. 30, iss. 5, pp. 1377–1424. ISSN 1433-3058. DOI: 10.1007/s00521-017-3295-y.
- [21] RAY, P. and D. P. MISHRA. Support vector machine based fault classification and location of a long transmission line. *Engineering Science and Technology, an International Journal*. 2016, vol. 19, iss. 3, pp. 1368–1380. ISSN 2215-0986. DOI: 10.1016/j.jestch.2016.04.001.
- [22] SANTOS D. and J. C. FERREIRA. IoT Power Monitoring System for Smart Environments. *Sustainability*. 2019, vol. 11, iss. 9, pp. 1–24. ISSN 2071-1050. DOI: 10.3390/su11195355.

- [23] BEDI, G., G. K. VENAYAGAMOORTHY, R. SINGH, R. R. BROOKS and K.-C. WANG. Review of Internet of Things (IoT) in Electric Power and Energy Systems. *IEEE Internet of Things Journal*. 2018, vol. 5, iss. 2, pp. 847–870. ISSN 2327-4662. DOI: 10.1109/JIOT.2018.2802704.
- [24] LIU, Q., Y. MA, M. ALHUSSEIN, Y. ZHANG and L. PENG. Green data center with IoT sensing and cloud-assisted smart temperature control system. *Computer Networks*. 2016, vol. 101, iss. 1, pp. 104–112. ISSN 1872-7069. DOI: 10.1016/j.comnet.2015.11.024.
- [25] SHEKAR, S. C., G. KUMAR and S. V. N. L. LALITHA. A transient current based micro-grid connected power system protection scheme using wavelet approach. *International Journal of Electrical and Computer Engineering*. 2019, vol. 9, iss. 1, pp. 14–22. ISSN 2722-2578. DOI: 10.11591/ijece.v9i1.pp14-22.
- [26] HE, Z., L. FU, S. LIN and Z. BO. Fault Detection and Classification in EHV Transmission Line Based on Wavelet Singular Entropy. *IEEE Transactions on Power Delivery*. 2010, vol. 25, iss. 4, pp. 2156–2163. ISSN 1937-4208. DOI: 10.1109/TPWRD.2010.2042624.
- [27] REDDY, M. J. B., D. V. RAJESH and D. K. MOHANTA. Robust transmission line fault classification using wavelet multi-resolution analysis. *Computers & Electrical Engineering*. 2013, vol. 39, iss. 4, pp. 1219–1247. ISSN 1879-0755. DOI: 10.1016/j.compeleceng.2013.02.013.
- [28] MISHRA, D. P. and P. RAY. Fault detection, location and classification of a transmission line. *Neural Computing and Applications*. 2018, vol. 30, iss. 5, pp. 1377–1424. ISSN 1433-3058. DOI: 10.1007/s00521-017-3295-y.

About Authors

Gantaiah Swamy GARICA (corresponding author) was born in Vijayawada, Andhra Pradesh, India. He received his M.Tech. Degree from National Institute of Technology, Calicut in 2007. Presently working as Assistant professor in Andhra Loyola Institute of Engineering and Technology, Vijayawada and pursuing Ph.D. in Andhra University. His research interests include transmission line protection, wavelets, IoT based protection schemes, microgrid.

Padma KOTTALA was born in Karnool, India. She received her Ph.D. from Andhra University in 2015. Presently working as Assistant Professor in

Andhra University, Visakhapatnam, Andhra Pradesh, India. Her research interests include Optimal location of FACTS Devices, power system optimisation algorithms, micro grid protection schemes.

Appendix A

1.1. Data Input Initialisation with MATLAB Code

The MATLAB code for the analysis of faults in the proposed system as follows: The following sample sequence of MATLAB code for zone-1 (Fig. 13).

1.2. Input Data Initialisation

```
iaZ1 = []; ibZ1 = []; icZ1 = []; iaZ11 = []; ibZ11 = []; icZ11 = [];
open('swami_wind_grk.slx');
for km1=10:10:110;
km2=130-km1;
ctr2=1; for tt=0.015625:0.0009765:0.0234375;
Ts1=1/1920;
Ts=1/192000;
sim('swami_wind_grk.slx');
```

1.3. Wave-Decomposition of Zone-1

```
[CiaZ1, LiaZ1] = wavedec(iaZ1, 1, 'bior - 1.5');
[CibZ1, LibZ1] = wavedec(ibZ1, 1, 'bior - 1.5');
[CicZ1, LicZ1] = wavedec(icZ1, 1, 'bior - 1.5');
[CiaZ11, LiaZ11] = wavedec(iaZ11, 1, 'bior - 1.5');
[CibZ11, LibZ11] = wavedec(ibZ11, 1, 'bior - 1.5');
[CicZ11, LicZ11] = wavedec(icZ11, 1, 'bior - 1.5');
```

1.4. Sample Detailed-Coefficients Calculation Code

```
CD1 - iaZ1 = detcoef(CiaZ1, LiaZ1, 1);
CD1 - ibZ1 = detcoef(CibZ1, LibZ1, 1);
CD1 - icZ1 = detcoef(CicZ1, LicZ1, 1);
CD1 - iaZ11 = detcoef(CiaZ11, LiaZ11, 1);
CD1 - ibZ11 = detcoef(CibZ11, LibZ11, 1);
CD1 - icZ11 = detcoef(CicZ11, LicZ11, 1);
```

1.5. Calculation of Impact Analysis of Faults

```
Zone1 - iaZ = (CD1 - iaZ1 - CD1 - iaZ11);
Zone1 - ibZ = (CD1 - ibZ1 - CD1 - ibZ11);
Zone1 - icZ = (CD1 - icZ1 - CD1 - icZ11);
```

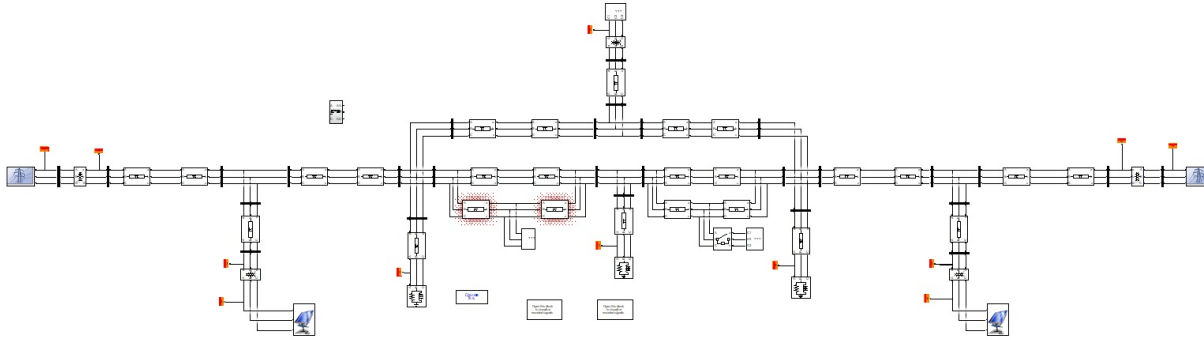


Fig. 13: Simulation diagram for wide area test system

1.6. Test Data Generation for ANN to Find the Location of Fault

$$\begin{aligned} \text{Zone1} - iaZ &= (CD1 - iaZ1); \\ \text{Zone1} - ibZ &= (CD1 - ibZ1); \\ \text{Zone1} - icZ &= (CD1 - icZ1); \end{aligned}$$

1.7. Preparation of Fault Index

$$\begin{aligned} \text{Sum1} - iaZ(i) &= CD1 - iaZ(i) + CD1 - iaZ(i+1) + \\ &CD1 - iaZ(i+2) + CD1 - iaZ(i+3) + CD1 - iaZ(i+4) + \\ &CD1 - iaZ(i+5) + CD1 - iaZ(i+6) + CD1 - iaZ(i+7); \\ \text{Sum1} - ibZ(i) &= CD1 - ibZ(i) + CD1 - ibZ(i+1) + \\ &CD1 - ibZ(i+2) + CD1 - ibZ(i+3) + CD1 - ibZ(i+4) + \\ &CD1 - ibZ(i+5) + CD1 - ibZ(i+6) + CD1 - ibZ(i+7); \\ \text{Sum1} - icZ(i) &= CD1 - icZ(i) + CD1 - icZ(i+1) + \\ &CD1 - icZ(i+2) + CD1 - icZ(i+3) + CD1 - icZ(i+4) + \\ &CD1 - icZ(i+5) + CD1 - icZ(i+6) + CD1 - icZ(i+7); \end{aligned}$$

1.8. Data Visualisation

$$\begin{aligned} \text{plot}(CD1 - iaZ, \text{xlabel}('Time - msec'), \text{ylabel}('z1 - \\ \text{Index} - iaZ')); \\ \text{plot}(CD1 - ibZ, \text{xlabel}('Time - msec'), \text{ylabel}('z1 - \\ \text{Index} - ibZ')); \\ \text{plot}(CD1 - icZ, \text{xlabel}('Time - msec'), \text{ylabel}('z1 - \\ \text{Index} - icZ')); \end{aligned}$$

$$\text{plot}(x, \text{Sum1} - iaZ, x, \text{Sum1} - ibZ, x, \text{Sum1} - icZ, x, y, ' - k'), \text{xlabel}('Time - msec'), \text{ylabel}('Z1 - Fault - Index');$$

$$\text{plot}(x, \text{Sum2} - iaZ, x, \text{Sum2} - ibZ, x, \text{Sum2} - icZ, x, y, ' - k'), \text{xlabel}('Time - msec'), \text{ylabel}('Z2 - Fault - Index');$$

$$\text{plot}(x, \text{Sum3} - iaZ, x, \text{Sum3} - ibZ, x, \text{Sum3} - icZ, x, y, ' - k'), \text{xlabel}('Time - msec'), \text{ylabel}('Z3 - Fault - Index');$$

$$\text{plot}(x, \text{Sum4} - iaZ, x, \text{Sum4} - ibZ, x, \text{Sum4} - icZ, x, y, ' - k'), \text{xlabel}('Time - msec'), \text{ylabel}('Z4 - Fault - Index');$$

$$\text{plot}(x, \text{Sum5} - iaZ, x, \text{Sum5} - ibZ, x, \text{Sum5} - icZ, x, y, ' - k'), \text{xlabel}('Time - msec'), \text{ylabel}('Z5 - Fault - Index');$$

$$\text{plot}(x, \text{Sum6} - iaZ, x, \text{Sum6} - ibZ, x, \text{Sum6} - icZ, x, y, ' - k'), \text{xlabel}('Time - msec'), \text{ylabel}('Z6 - Fault - Index');$$

1.9. Data Extraction for Implementing SVM

$$\begin{aligned} \text{xlswrite}('zone4/Pv - hvdc - Z4 - AG', \text{Indx} - a1 - 11, 'Zone1 - a'); \\ \text{xlswrite}('zone4/Pv - hvdc - Z4 - AG', \text{Indx} - b1 - 11, 'Zone1 - b'); \\ \text{xlswrite}('zone4/Pv - hvdc - Z4 - AG', \text{Indx} - c1 - 11, 'Zone1 - c'); \end{aligned}$$